

## Data reduction of the $^{18}\text{O} + ^{48}\text{Ti}$ elastic and inelastic scattering at 275 MeV in the context of the NUMEN project

G. A. BRISCHETTO<sup>(1)(2)</sup> on behalf of the NUMEN COLLABORATION

<sup>(1)</sup> *Dipartimento di Fisica e Astronomia, Università degli Studi di Catania - Catania, Italy*

<sup>(2)</sup> *INFN, Laboratori Nazionali del Sud - Catania, Italy*

received 31 January 2022

**Summary.** — The  $^{18}\text{O} + ^{48}\text{Ti}$  reaction at 275 MeV bombarding energy was studied at the INFN-LNS within the framework of the NUMEN project. The elastic and inelastic scattering channels were measured using the MAGNEX magnetic spectrometer with the aim of extracting the initial-state interaction of the involved nuclei. The ray reconstruction method was applied to the experimental data to obtain the scattering angles and the momentum vectors of the ejectiles, at the target point.

### 1. – Introduction

The possible connection between the Double Charge Exchange (DCE) reactions and the neutrinoless double beta decay ( $0\nu\beta\beta$ ) has opened new and interesting scenarios both from a theoretical and experimental point of view [1,2]. The NUMEN (NUclear Matrix Elements for Neutrinoless double beta decay) project [3-5] at Laboratori Nazionali del Sud of Istituto Nazionale di Fisica Nucleare (INFN-LNS) was proposed with the main goal of extracting data-driven information about the Nuclear Matrix Elements (NMEs) of the  $0\nu\beta\beta$  by measuring the cross-sections of heavy-ion induced DCE reactions. In order to extract the NMEs from experimental cross-sections, an accurate description of the reaction mechanism is mandatory. To this aim, the knowledge of the initial and final state interaction of the reactions of interest is very important, because they express the distortion of the incoming and outgoing waves generated by the optical potential, which describes the average interaction between the involved nuclei. The analysis of the elastic scattering channel is the usual way to access the relevant optical potential. In the following, the data reduction for the  $^{18}\text{O} + ^{48}\text{Ti}$  elastic and inelastic scattering at 15.3 A MeV is shown.

### 2. – Experimental setup

The  $^{18}\text{O}^{8+}$  beam was delivered at 275 MeV by the K800 superconducting cyclotron of the INFN-LNS facility in Catania. The target was a foil of  $\text{TiO}_2$  510  $\mu\text{g}/\text{cm}^2$  thick, which

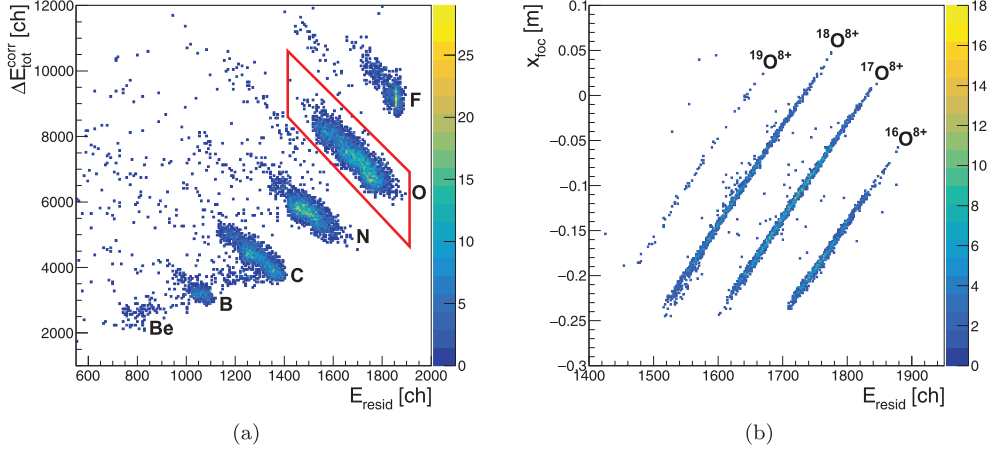


Fig. 1. – (a) Typical  $\Delta E$ - $E_{resid}$  plot for a single silicon detector at  $\theta_{opt} = 9^\circ$ . (b)  $x_{foc}$ - $E_{resid}$  plot for the ions selected with the graphical cut in (a).

was evaporated on a  $216 \mu\text{g}/\text{cm}^2$  aluminum backing. To estimate the background coming from the main target contaminants, measurements with both an aluminum and a  $\text{WO}_3$  target were also performed. The scattered  $^{18}\text{O}$  ejectiles were analyzed in momentum by the MAGNEX large acceptance magnetic spectrometer [6] and measured by the Focal Plane Detector (FPD) [7]. The experimental data were collected in three separate runs, where the MAGNEX optical axis ( $\theta_{opt}$ ) was set at  $9^\circ$ ,  $15^\circ$ , and  $21^\circ$  with respect to the beam direction. In the first angular configuration, the spectrometer worked in full horizontal acceptance, while the vertical one was reduced. In the other two cases, the MAGNEX acceptance was set to its maximum value of 50 msr.

### 3. – Data reduction

The starting point of the data reduction procedure is an accurate selection of the  $^{18}\text{O}^{8+}$  ions, which is obtained through the use of two techniques, as described in ref. [8]. The atomic number ( $Z$ ) identification is accomplished with the standard  $\Delta E$ - $E$  method, where the  $\Delta E$  parameter is properly corrected for the measured trajectory angle: as highlighted in fig. 1(a), the atomic species between the beryllium and the fluorine are clearly distinguishable. After selecting the relevant ion with a graphical cut, the mass identification is performed in terms of the mass-to-charge ( $\sqrt{m}/q$ ) ratio by using a technique based on the correlation between the horizontal coordinate of the ejectile at the focal plane ( $x_{foc}$ ) and its residual energy ( $E_{resid}$ ). In fig. 1(b), the two-dimensional  $x_{foc}$ - $E_{resid}$  plot for the selected ions in fig. 1(a) is reported. As can be seen, the mass resolution of MAGNEX (about 1/300) allows a sharp identification of the  $^{18}\text{O}^{8+}$  isotope.

After the particle identification, an algorithm based on the COSY INFINITY software [9] is applied to the data in order to reconstruct the ejectile trajectories and deduce the momentum vector at the target position. Because of the aberrations typical of a large acceptance spectrometer, the equations of motion of the ions are solved to the 10th order. Feeding COSY INFINITY with the magnetic and geometric setup of the experiment, the direct transport operator is built. It connects the initial phase-space parameters to the final ones. The reliability of the reconstructed transport matrix is tested by comparing

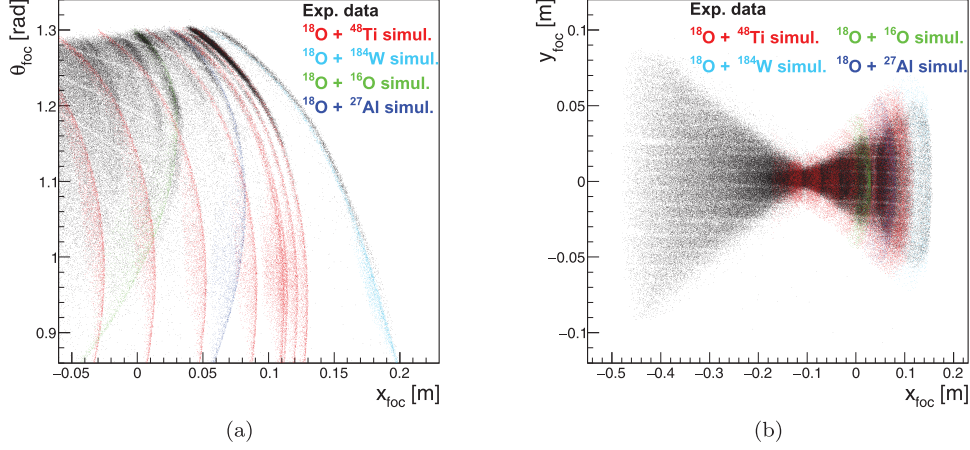


Fig. 2. – (a) Horizontal final phase-space representation in terms of the  $\theta_{foc}$ - $x_{foc}$  parameters for both the experimental and simulated data at  $\theta_{opt} = 15^\circ$ . (b) Vertical final phase-space representation in terms of the  $y_{foc}$ - $x_{foc}$  parameters for both the experimental and simulated data at  $\theta_{opt} = 15^\circ$ .

the final phase-space observables measured at the FPD with simulated events generated with an algorithm based on Monte Carlo methods. The software takes into account the relativistic kinematics and the excitation energies of the ejectiles and of the residual nuclei, thus allowing to simulate not only ground-state to ground-state processes, but also transitions to excited states. A fine tuning of the magnetic fields at the boundary regions of the bending magnet is performed in order to optimize the agreement between the experimental and the simulated data. In fig. 2(a), the horizontal representation of the final phase-space, expressed in terms of the correlation between the horizontal angle ( $\theta_{foc}$ ) and  $x_{foc}$ , is shown for both the experimental and simulated data.

In the experimental data, the most intense loci correspond to the  $^{18}\text{O} + ^{48}\text{Ti}$  elastic and inelastic scattering. Other loci are visible in the plot, due to the scattering of  $^{18}\text{O}$  on W, Al, and O, present in the target and the backing. The simulated data include both elastic scattering events and inelastic transitions to the low-lying excited states of  $^{18}\text{O}$  and  $^{48}\text{Ti}$ . The  $^{18}\text{O}$  elastic scattering on W, O, and Al is also simulated. To explore the spectrometer response in the full range of accepted momenta, fictitious excited states with energy ranging from 0 and 20 MeV are also taken into account. In fig. 2(b), the vertical representation of the final phase-space, in terms of the vertical coordinate ( $y_{foc}$ ) and  $x_{foc}$ , is illustrated for both the experimental and simulated data. The *butterfly shape* of the experimental data is typical of a quadrupole-dipole large acceptance spectrometer like MAGNEX, where the trajectories are vertically focused for few  $x_{foc}$  values. At large  $x_{foc}$  values it is possible to recognize the locus originated by the elastic scattering of  $^{18}\text{O}$  off the W contaminant. The good overlap between experimental and simulated data for both the horizontal and the vertical component of the final phase-space parameters confirms the reliability of the adopted direct transport operator. The latter is then inverted by COSY INFINITY, producing the inverse transport map, which allows reconstructing the initial phase-space parameters starting from the final phase-space observables measured at the FPD.

Once the initial phase-space parameters are known, the laboratory scattering an-

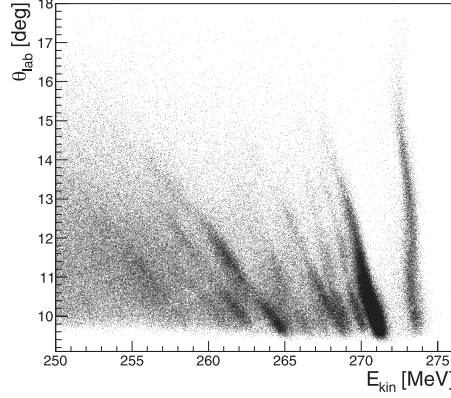


Fig. 3. – The  $\theta_{lab}$ - $E_{kin}$  spectrum at  $\theta_{opt} = 15^\circ$ .

gles ( $\theta_{lab}$ ) and the initial kinetic energies ( $E_{kin}$ ) of the ejectiles can be deduced. The correlation spectrum between these two parameters is shown in fig. 3. The loci corresponding to the  $^{18}\text{O} + ^{48}\text{Ti}$  scattering have a characteristic slope that is due to the relation between the kinetic energy and the scattering angle. At higher energy values, the kinematic locus of the scattering of the  $^{18}\text{O}$  off the W contaminant is evident. This preliminary analysis shows that the trajectory reconstruction technique is valid and that the reconstructed parameters are reasonable.

#### 4. – Conclusions

In the framework of the NUMEN project, the  $^{18}\text{O} + ^{48}\text{Ti}$  elastic and inelastic scattering was measured at the INFN-LNS. The scattered nuclei were analyzed in momentum by the MAGNEX magnetic spectrometer and detected by the Focal Plane Detector. Once the particle identification was performed, the ray reconstruction procedure was applied to the experimental data to extract the scattering parameters at the target position. In the next steps of the analysis, the elastic and inelastic absolute cross-section angular distributions will be deduced and compared to theoretical calculations [10-13].

#### REFERENCES

- [1] SANTOPINTO E. *et al.*, *Phys. Rev. C*, **98** (2018) 061601(R).
- [2] LENSKE H. *et al.*, *Prog. Part. Nucl. Phys.*, **109** (2019) 103716.
- [3] CAPPUZZELLO F. *et al.*, *Eur. Phys. J. A*, **54** (2018) 72.
- [4] AGODI C. *et al.*, *Universe*, **7** (2021) 72.
- [5] CAPPUZZELLO F. *et al.*, *Int. J. Mod. Phys. A*, **36** (2021) 2130018.
- [6] CAPPUZZELLO F. *et al.*, *Eur. Phys. J. A*, **52** (2016) 167.
- [7] TORRESI D. *et al.*, *Nucl. Instrum. Methods A*, **989** (2021) 164918.
- [8] CAPPUZZELLO F. *et al.*, *Nucl. Instrum. Methods A*, **621** (2010) 419.
- [9] MAKINO K. *et al.*, *Nucl. Instrum. Methods A*, **427** (1999) 338.
- [10] CARBONE D. *et al.*, *Universe*, **7** (2021) 58.
- [11] CAVALLARO M. *et al.*, *Front. Astron. Space Sci.*, **8** (2021) 659815.
- [12] LA FAUCI L. *et al.*, *Phys. Rev. C*, **104** (2021) 054610.
- [13] SPATAFORA A. *et al.*, *Phys. Rev. C*, **100** (2019) 034620.